

AN INVESTIGATION ON THE BUCKLING ANALYSIS OF SMART FUNCTIONALLY GRADED CIRCULAR PLATE WITH PIEZOELECTRIC PROPERTIES UNDER OUT OF PLANE PERIODIC ELECTRIC FIELD AND UNIFORM RADIAL COMPRESSIVE EDGE LOADING

F. Ebrahimi^{1*}

¹Mechanical Engineering department, Faculty Of Engineering, Imam Khomeini International University, Qazvin, Iran

ABSTRACT

The buckling analysis of a solid circular functionally graded piezoelectric plate subjected to the uniform radial compressive edge loading and an out of plane periodic electric field is presented. The material properties of the FGPM plate are assumed to vary continuously through the thickness of the plate according to a power law distribution of the volume fraction of the constituent materials. The general mechanical nonlinear equilibrium and stability equations are derived using the variational formulations to obtain the governing equations of the smart FG plate and dynamic instability regions are obtained employing the Bolotin's method. Several important aspects such as applied electric field, mechanical loading and different plate thickness ratios as well as the FG volume fraction exponent which have impacts on critical buckling load and free vibration frequency rate of piezoelectric circular plate are investigated and discussed in detail. Numerical results are tabulated in several tables and figures. It is revealed that the piezoelectricity affects the unstable region slightly whilst the functionally graded composite material plays a significant role in changing the unstable regions and the buckling loads of the smart plate.

KEYWORDS: *Solid circular plate; Buckling analysis; Piezoelectric functionally graded plate*

1.0 INTRODUCTION

Smart piezoelectric sensors and actuators have been widely used in micro-electro-mechanical systems (MEMS). Typical piezoelectric bending actuators involve multilayer stacks and make use of the flexural deformation mode to produce larger deflections. However, the chief disadvantage of conventional layered piezoelectric actuators is that the bonding agent may crack at low temperature and creep or peel

* Corresponding author email: febrahimi@eng.ikiu.ac.ir

off at high temperature (Zhu & Meng, 1995). Another disadvantage is that they suffer stress concentration near the interlayer surfaces due to the abrupt changes in both their material composition and thermo-electro-elastic properties, which can cause severe deterioration in both the interlayer bonding strength and the response performance (Lee, 2005). These drawbacks reduce the electrical field induced displacement characteristics, lifetime and reliability of piezoelectric bimorph actuators, and also restrict the utility of piezoelectric actuators in the area of measured devices requiring high reliability. To solve these problems, Zhu and Meng (1995) reported the fabrication of a functionally graded piezoelectric material (FGPM) actuator by using the powder mold stacking press method and discussed the experimental measurement of the displacement characteristics and compositional distribution of these actuators. The novel actuator with material coefficients varying smoothly along the layer thickness was sandwiched between distinct piezoelectric layers. Functionally graded materials (FGMs) have attracted much attention as advanced structural materials because of their heat-resistance properties. An advantage of a functionally graded (FG) plate over a laminated plate is that material properties vary continuously through the plate thickness, thus no sudden discontinuities in stresses occur across an interface between any two adjoining laminate thereby eliminating the delamination mode of failure. FGMs are usually made of a mixture of ceramic and metal, and can thus resist high-temperature conditions while maintaining toughness. The metal-ceramic composite plates are widely used in aircrafts, space vehicles, reactor vessels and other engineering applications. Unlike fiber-matrix composites, in which cracking and debonding may occur at high temperatures due to the material property mismatch at the interface of two discrete materials, FGMs have the advantage of being capable of withstanding severe high temperature while maintaining structural integrity. Due to this superior thermo-mechanical property, FGM plate structures have found a wide range of applications in many industries, especially in space vehicles and aircrafts, where they are very often subjected to high levels of thermal and dynamic loading, such as large temperature gradients and acoustic pressure. This may result in complicated stability and buckling behavior of the FGM plate due to the bending-stretching coupling and combined external loads. Hence, it is of prime importance to understand the buckling behavior of FGM plate structures. The piezoelectric materials have coupled effects between the elastic field and the electric field. Due to the widespread use of the piezoelectric materials in sensors and actuators, the study of embedded or surface-mounted piezoelectric materials has received considerable attention in recent years. There is a special interest in the modeling for piezoelectric coupled circular and annular plates since

piezoelectric material can be used as actuator in ultrasonic motor (Yamaguchi et al., 2013) in response to the need for a lightweight, high-torque and low-speed motor for fractional horsepower applications. It is based on the concept of driving a rotor by mechanical vibration excited by piezoelectric patch on a stator via piezoelectric effect (Zhao, 2011). When a periodic loading acts on the plane of a plate, it is well known that under some circumstances the ordinary forced response will become dynamically unstable, leading to an intense vibration, which is called the dynamic instability phenomenon. The stability problem for plates was solved first by Bodner (1938) applying series and Galerkin methods. By geometrically nonlinear formulation with accounting of energy dissipation, Bažant et al. (2010) presented the dynamic stability of structures like plates under various conditions like elastic, inelastic, fracture and also presented the damage theories. Many studies for free vibration and transient response of FGMs are available in the literature. Hosseini-Hashemi et al. (2011) presented an exact analytical approach for free vibration analysis of functionally graded rectangular plates. Efraim and Eisenberger (2007) derived the equations of motion including the effect of shear deformations using the first-order shear deformation theory, and solved exactly for various combinations of boundary conditions. By using the method of power series expansion of displacement components, Matsunaga (2008) derived a set of fundamental dynamic equations of a two-dimensional (2-D) higher-order theory for rectangular functionally graded (FG) plates through Hamilton's principle. Zhao et al. (2009) analyzed free vibration of metal and ceramic functionally graded plates that uses the element-free kp-Ritz method.

Although there is a considerable interest in investigating the performance and the behavior of FGM plates coupled with piezoelectric actuators, very limited research work is available on stability analysis of functionally graded piezoelectric plates. Koizumi (1993) first proposed the concept of FGM. Ebrahimi and Rastgoo presented an analytical solution for the free axisymmetric vibration of piezoelectric coupled thin circular (Ebrahimi & Rastgo, 2008a) and thin annular (Ebrahimi & Rastgo, 2008b) FGM plates. They also presented a theoretical analysis of smart moderately thick shear deformable annular (Ebrahimi et al., 2009) and circular (Ebrahimi et al., 2008) functionally graded plate by using Mindlin's plate theory. The nonlinear free and forced vibration behavior of functionally graded plate with piezoelectric layers in thermal environment was studied by Fakhari et al. (2011). Khorshidvand et al. (2012) theoretically investigated the thermoelastic buckling of functionally graded circular plates integrated with piezoelectric layers and a B-spline finite strip method for sandwich FGM plate structures

coupled with piezoelectric skins was proposed by Loja et al. (2013). Most recently Ebrahimi (2013) investigated analytically the vibrations and dynamic response of functionally graded plate integrated with piezoelectric layers in thermal environment.

To the author's best knowledge and according to the comprehensive literature survey, there is no work reported on the study of the dynamic stability of FGPM circular plates, so the main contribution of this paper is to present an analytical solution to the problem of dynamic stability of piezoelectric circular plates with functionally graded microstructure. The aim of the present paper is to derive the dynamic instability region of functionally graded piezoelectric circular plates from combination of variations and adjacent-equilibrium criterion and Bolotin's method. Then a solution for the FG piezoelectric circular plates subjected to uniform compression loads is obtained. The effect of plate parameters such as thickness-radius ratios, power index, as well as electric field and mechanical loads on instability behavior of the plate is comprehensively investigated.

2.0 THEORY AND FORMULATION

The functionally graded piezoelectric circular plate is assumed to be of radius R and thickness h . The material effective properties of the plate can be expressed as (Ebrahimi, 2013)

$$P_{eff} = P_u + (P_b - P_u)(z/h + 1/2)^n \quad (1)$$

where P_{eff} is the effective material property of the functionally gradient material, P_u and P_b are the dependent properties of the top and bottom surfaces of the plate, respectively. The fraction index n dictates the material variation profile through the plate thickness and may be varied to obtain the optimum distribution of component materials. From Equation (1) the effective Young's modulus, E , mass density, ρ , piezoelectric stress constants, e_{ij} , and dielectric constants, ξ_{ij} , of an FGM piezoelectric plate can be written as

$$(E, \rho, e_{ij}, \xi_{ij}) = (E, \rho, e_{ij}, \xi_{ij})_u + ((E, \rho, e_{ij}, \xi_{ij})_b - (E, \rho, e_{ij}, \xi_{ij})_u)(z/h + 1/2)^n \quad (2)$$

The FG piezoelectric circular plate considered in this study is subjected to uniform radial compressive loading p_r along its edge and periodic electric field E in the out-plane direction by

$$\begin{aligned} p_r &= p_0 + p_t \cos \omega t \\ E_z &= E_{z0} + E_{zt} \cos \omega t \end{aligned} \tag{3}$$

The constitutive equations of a FG piezoelectric material in two dimensional strain-stress law for plane-stress condition are given by

$$\begin{Bmatrix} \sigma_{rr} \\ \sigma_{\theta\theta} \\ \sigma_{r\theta} \end{Bmatrix} = E \begin{bmatrix} 1 & \nu & 0 \\ 1-\nu^2 & 1-\nu^2 & 0 \\ \nu & 1 & 0 \\ 0 & 0 & \frac{1}{2(1+\nu)} \end{bmatrix} \begin{Bmatrix} \varepsilon_{rr} \\ \varepsilon_{\theta\theta} \\ \varepsilon_{r\theta} \end{Bmatrix} - \begin{bmatrix} 0 & 0 & e_{31} \\ 0 & 0 & e_{32} \\ 0 & 0 & 0 \end{bmatrix} \begin{Bmatrix} 0 \\ 0 \\ E_z \end{Bmatrix} \tag{4}$$

$$\begin{Bmatrix} D_r \\ D_\theta \\ D_z \end{Bmatrix} = \begin{bmatrix} 0 & 0 & 0 \\ 0 & 0 & 0 \\ e_{31} & e_{31} & 0 \end{bmatrix} \begin{Bmatrix} \varepsilon_{rr} \\ \varepsilon_{\theta\theta} \\ \varepsilon_{r\theta} \end{Bmatrix} + \begin{bmatrix} \xi_{11} & 0 & 0 \\ 0 & \xi_{22} & 0 \\ 0 & 0 & \xi_{33} \end{bmatrix} \begin{Bmatrix} 0 \\ 0 \\ E_z \end{Bmatrix} \tag{5}$$

where $\{\sigma\}$ is the stress vector, $\{D\}$ is the electrical displacement vector, the Poisson's ratio ν is assumed to be constant across the plate thickness. According to the Love-Kirchhoff assumptions, we get

$$\begin{Bmatrix} \varepsilon_{rr} \\ \varepsilon_{\theta\theta} \\ \varepsilon_{r\theta} \end{Bmatrix} = \begin{Bmatrix} \bar{\varepsilon}_{rr} \\ \bar{\varepsilon}_{\theta\theta} \\ \bar{\varepsilon}_{r\theta} \end{Bmatrix} + z \begin{Bmatrix} k_{rr} \\ k_{\theta\theta} \\ k_{r\theta} \end{Bmatrix} = \begin{Bmatrix} u_r + w_r^2/2 \\ v_{,\theta}/r + u/r + (w_{,\theta}/2)^2 \\ u_{,\theta}/r + v_r - v/r + (w_r/r)w_{,\theta} \end{Bmatrix} + z \begin{Bmatrix} -w_{,rr} \\ -w_{,r}/r - w_{,\theta\theta}/r^2 \\ -2(w_{,r\theta}/r - w_{,\theta}/r^2) \end{Bmatrix} \tag{6}$$

where $\bar{\varepsilon}_{rr}$, $\bar{\varepsilon}_{\theta\theta}$ and $\bar{\varepsilon}_{r\theta}$, and are the engineering strain components in the median surface, k_{rr} , $k_{r\theta}$ and $k_{\theta\theta}$ are the curvatures which can be expressed in terms of the displacement components, u , v and w represent the corresponding components of the displacement of a point on the middle plate surface. In the following deduction, applying Hamilton's principle while deriving the dynamic equation for the FGM piezoelectric circular plate, it can be expressed as

$$\delta \int_{t_1}^{t_2} V - \delta \int_{t_1}^{t_2} [U + W - T] dt = 0 \tag{7}$$

where δ is the first variation operator, V is the total energy, T is the kinetic energy, U is the potential energy, W is the work done by the periodic edge loading p_r . It is well knew that

$$U = \frac{1}{2} \int_0^r \int_0^{2\pi} \int_{-h/2}^{h/2} (\varepsilon_{ij} \sigma_{ij} + D_{ij} E_{ij}) r dr d\theta dz \tag{8}$$

$$W = - \int_0^r \int_0^{2\pi} p_r u_r r dr d\theta \tag{9}$$

$$T = \frac{1}{2} \int_0^r \int_0^{2\pi} \int_{-h/2}^{h/2} \rho w_t^2 r dr d\theta dz \tag{10}$$

Substituting Equations (4), (5) and (6) into Equation (7), integrating with respect to z from $-h/2$ to $h/2$, the total energy now gives

$$V = \iint F dr d\theta \tag{11}$$

where

$$F = r \left\{ \frac{A}{2(1-\nu^2)} \left(\bar{\varepsilon}_{rr}^2 + \bar{\varepsilon}_{\theta\theta}^2 + 2\nu \bar{\varepsilon}_{rr} \bar{\varepsilon}_{\theta\theta} + \frac{1-\nu}{2} \bar{\varepsilon}_{r\theta}^2 \right) + \frac{B}{2(1-\nu^2)} \left(k_{rr}^2 + k_{\theta\theta}^2 + 2\nu k_{rr} k_{\theta\theta} + \frac{1-\nu}{2} k_{r\theta}^2 \right) + \frac{C}{1-\nu^2} \left(\bar{\varepsilon}_{rr} k_{rr} + \bar{\varepsilon}_{\theta\theta} k_{\theta\theta} + \nu (\bar{\varepsilon}_{rr} k_{\theta\theta} + \bar{\varepsilon}_{\theta\theta} k_{rr}) + \frac{1-\nu}{2} \bar{\varepsilon}_{r\theta} k_{r\theta} \right) + \frac{1}{2} \int_{-h/2}^{h/2} \varepsilon_{33} E_z^2 dz + \frac{1}{2} \int_{-h/2}^{h/2} \rho w_t^2 dz - p_r u_r \right\} \tag{12}$$

and

$$(A, B, C) = \int_{-h/2}^{h/2} E(1, z^2, z) dz \tag{13}$$

According Hamilton’s principle, the integrand F must satisfy the Euler equations of the calculus of variations. Results in the dynamic equilibrium equations in terms of the functional F as

$$\begin{aligned} \frac{\partial F}{\partial u} - \frac{\partial}{\partial r} \frac{\partial F}{\partial u_r} - \frac{\partial}{\partial \theta} \frac{\partial F}{\partial u_{,\theta}} &= 0 \\ \frac{\partial F}{\partial v} - \frac{\partial}{\partial r} \frac{\partial F}{\partial v_r} - \frac{\partial}{\partial \theta} \frac{\partial F}{\partial v_{,\theta}} &= 0 \\ \frac{\partial F}{\partial w} - \frac{\partial}{\partial r} \frac{\partial F}{\partial w_r} - \frac{\partial}{\partial \theta} \frac{\partial F}{\partial w_{,\theta}} - \frac{\partial}{\partial t} \frac{\partial F}{\partial w_t} + \frac{\partial^2}{\partial r^2} \frac{\partial F}{\partial w_{,rr}} + \frac{\partial^2}{\partial r \partial \theta} \frac{\partial F}{\partial w_{,r\theta}} + \frac{\partial^2}{\partial \theta^2} \frac{\partial F}{\partial w_{,\theta\theta}} &= 0 \end{aligned} \tag{14}$$

substituting Equations (6) and (12) into Equation (14), the dynamic equilibrium equations for general circular plate composed of FG piezoelectric material are given by

$$\begin{aligned}
 N_{r,r} + \frac{1}{r}N_{r\theta,\theta} + \frac{N_r - N_\theta}{r} &= 0 \\
 N_{r\theta,r} + \frac{1}{r}N_{\theta,\theta} + \frac{2}{r}N_{r\theta} &= 0 \\
 \frac{\partial}{\partial \theta}(N_\theta w_{,\theta} + N_{r\theta} w_{,r}) + \frac{\partial}{\partial r}(rN_r w_{,r} + N_{r\theta} w_{,\theta}) - \frac{\partial}{\partial r}M_\theta + \frac{\partial}{\partial \theta}\left(\frac{2M_{r\theta}}{r}\right) \\
 + \frac{\partial^2}{\partial r^2}(rM_r) + \frac{\partial^2}{\partial r \partial \theta}(2M_{r\theta}) + \frac{\partial^2}{\partial \theta^2}\left(\frac{M_\theta}{r}\right) + \frac{\partial}{\partial r} \int_{-h/2}^{h/2} e_{31} E_z w_{,r} r dz - \frac{\partial}{\partial r} \int_{-h/2}^{h/2} e_{31} E_z z dz \\
 - \frac{\partial}{\partial \theta} \int_{-h/2}^{h/2} \frac{e_{31} E_z w_{,\theta}}{r} dz + \frac{\partial^2}{\partial r^2} \int_{-h/2}^{h/2} r e_{31} E_z z dz + \frac{\partial^2}{\partial \theta^2} \int_{-h/2}^{h/2} \frac{e_{31} E_z z}{r} dz + \int_{-h/2}^{h/2} \rho w_{,tt} r dz = 0
 \end{aligned} \tag{15}$$

where

$$\begin{Bmatrix} (N_r, M_r) \\ (N_\theta, M_\theta) \\ (N_{r\theta}, M_{r\theta}) \end{Bmatrix} = \frac{(A,C)}{1-\nu^2} \begin{bmatrix} 1 & \nu & 0 \\ \nu & 1 & 0 \\ 0 & 0 & \frac{1-\nu}{2} \end{bmatrix} \begin{Bmatrix} \bar{\epsilon}_{rr} \\ \bar{\epsilon}_{\theta\theta} \\ \bar{\epsilon}_{r\theta} \end{Bmatrix} + \frac{(C,B)}{1-\nu^2} \begin{bmatrix} 1 & \nu & 0 \\ \nu & 1 & 0 \\ 0 & 0 & \frac{1-\nu}{2} \end{bmatrix} \begin{Bmatrix} k_{rr} \\ k_{\theta\theta} \\ k_{r\theta} \end{Bmatrix} - \int_{-h/2}^{h/2} \begin{Bmatrix} e_{31} \\ e_{31} \\ 0 \end{Bmatrix} E_z(1,z) dz \tag{16}$$

Introduction of the appropriate constitutive relations for the moment intensities and rotations reduces the third of Equation (15), the dynamic equation for the FGM piezoelectric circular plate can be derived as

$$\begin{aligned}
 N_{r,r} + \frac{1}{r}N_{r\theta,\theta} + \frac{N_r - N_\theta}{r} &= 0 \\
 N_{r\theta,r} + \frac{1}{r}N_{\theta,\theta} + \frac{2}{r}N_{r\theta} &= 0 \\
 \frac{B}{1-\nu^2} \nabla^4 w - \left[N_r w_{,rr} + N_\theta \left(\frac{w_{,r}}{r} + \frac{w_{,\theta\theta}}{r^2} \right) + 2N_{r\theta} \left(-\frac{w_{,\theta}}{r^2} + \frac{w_{,r\theta}}{r} \right) \right] \\
 + \frac{C}{1-\nu^2} \left(-\frac{v_{,\theta}}{r^3} + \frac{v_{,r\theta}}{r^2} + \frac{u_{,r}}{r^2} - \frac{u}{r^3} - \frac{2u_{,rr}}{r} - \frac{u_{,\theta\theta}}{r^3} - \frac{u_{,r\theta\theta}}{r^2} - \frac{u_{,rr\theta}}{r} - \frac{v_{,\theta\theta\theta}}{r^3} - u_{,rrr} \right) \\
 - \nabla^2 w \int_{-h/2}^{h/2} e_{31} E_z dz + w_{,tt} \int_{-h/2}^{h/2} \rho dz = 0
 \end{aligned} \tag{17}$$

where

$$\nabla^2 = \frac{1}{r} \frac{\partial}{\partial r} \left(r \frac{\partial}{\partial r} \right) + \frac{1}{r^2} \frac{\partial^2}{\partial \theta^2}$$

3.0 STABILITY EQUATIONS

The dynamic stability equations of thin FG piezoelectric circular plate are derived using the adjacent-equilibrium criterion (Love, 2013). Let

$$\begin{aligned}
 u &\rightarrow u_0 + u_1 & N_r &\rightarrow N_{r0} + \Delta N_r \\
 v &\rightarrow v_0 + v_1 & N_\theta &\rightarrow N_{\theta0} + \Delta N_\theta \\
 w &\rightarrow w_0 + w_1 & N_{r\theta} &\rightarrow N_{r\theta0} + \Delta N_{r\theta}
 \end{aligned}
 \tag{18}$$

where the incremental displacement (u_1, v_1, w_1) is arbitrarily small and, tentatively, (u_0, v_0, w_0) and (u, v, w) are any two adjacent equilibrium configurations. The term with 0 subscripts correspond to the u_0, v_0, w_0 displacement, and the $\Delta N_r, \Delta N_\theta, \Delta N_{r\theta}$ are increments corresponding to u_1, v_1, w_1 . Let $N_{r1}, N_{\theta1}$ and $N_{r\theta1}$ represent the parts of $\Delta N_r, \Delta N_\theta$ and $\Delta N_{r\theta}$ respectively, that are linear in u_1, v_1, w_1 . For example, from Equations (6) and (16), we have

$$\begin{aligned}
 N_r + \Delta N_r &= \frac{A}{1-\nu^2} \left\{ u_{0,r} + \frac{(w_0 + w_1)^2}{2} + \nu \left(\frac{v_{0,\theta}}{r} + \frac{u_0}{r} + \frac{(w_0 + w_1)^2}{2r^2} \right) \right\} + \left[u_{1,r} + \nu \left(\frac{v_{1,\theta}}{r} + \frac{u_1}{r} \right) \right] \\
 &+ \frac{C}{1-\nu^2} \left\{ -w_{0,rr} + \nu \left(-\frac{w_{0,\theta}}{r} - \frac{w_{0,\theta\theta}}{r^2} \right) \right\} + \left[-w_{1,rr} + \nu \left(-\frac{w_{1,\theta}}{r} - \frac{w_{1,\theta\theta}}{r^2} \right) \right] - \int_{-h/2}^{h/2} e_{31} E_z dz = 0
 \end{aligned}
 \tag{19}$$

Eliminating the high order item, and considering w_0 and its derivatives are equal to zero for in-plane edge loading, therefore

$$\begin{aligned}
 N_{r0} &= \frac{A}{1-\nu^2} \left[u_{0,r} + \nu \left(\frac{v_{0,\theta}}{r} + \frac{u_0}{r} \right) \right] - \int_{-h/2}^{h/2} e_{31} E_z dz \\
 \Delta N_r &= \frac{A}{1-\nu^2} \left[u_{1,r} + \frac{w_{1,r}^2}{2} + \nu \left(\frac{v_{1,\theta}}{r} + \frac{u_1}{r} + \frac{w_{1,\theta}^2}{2r^2} \right) \right] + \frac{C}{1-\nu^2} \left[-w_{1,rr} + \nu \left(-\frac{w_{1,\theta}}{r} - \frac{w_{1,\theta\theta}}{r^2} \right) \right] \\
 N_{r1} &= \frac{A}{1-\nu^2} \left\{ \left[u_{1,r} + \nu \left(\frac{v_{1,\theta}}{r} + \frac{u_1}{r} \right) \right] + \frac{C}{1-\nu^2} \left[-w_{1,rr} + \nu \left(-\frac{w_{1,\theta}}{r} - \frac{w_{1,\theta\theta}}{r^2} \right) \right] \right\}
 \end{aligned}
 \tag{20}$$

then introduce into Equation (17), and omit the high order penny item, we arrive at the following equations governing the dynamic stability of the FG piezoelectric circular plate, that is

$$\begin{aligned}
 N_{r1,r} + \frac{1}{r} N_{r\theta1,\theta} + \frac{N_{r1} - N_{\theta1}}{r} &= 0 \\
 N_{r\theta1,r} + \frac{1}{r} N_{\theta1,\theta} + \frac{2}{r} N_{r\theta1} &= 0 \\
 \frac{B}{1-\nu^2} \nabla^4 w_1 - \left[N_{r0} w_{1,rr} + N_{\theta0} \left(\frac{w_{1,r}}{r} + \frac{w_{1,\theta\theta}}{r^2} \right) + 2N_{r\theta0} \left(-\frac{w_{1,\theta}}{r^2} + \frac{w_{1,r\theta}}{r} \right) \right] \\
 + \frac{C}{1-\nu^2} \left(-\frac{v_{1,\theta}}{r^3} + \frac{v_{1,r\theta}}{r^2} + \frac{u_{1,r}}{r^2} - \frac{u_1}{r^3} - \frac{2u_{1,rr}}{r} - \frac{u_{1,\theta\theta}}{r^3} - \frac{u_{1,r\theta\theta}}{r^2} - \frac{u_{1,rr\theta}}{r} - \frac{v_{1,\theta\theta\theta}}{r^3} - u_{1,rrr} \right) \\
 - \nabla^2 w_1 \int_{-h/2}^{h/2} e_{31} E_z dz + w_{1,tt} \int_{-h/2}^{h/2} \rho dz &= 0
 \end{aligned}
 \tag{21}$$

where

$$\begin{Bmatrix} N_{r0} \\ N_{\theta0} \\ N_{r\theta0} \end{Bmatrix} = \frac{1}{1-\nu^2} \begin{bmatrix} 1 & \nu & 0 \\ \nu & 1 & 0 \\ 0 & 0 & \frac{1-\nu}{2} \end{bmatrix} \begin{Bmatrix} Au_{0,r} \\ A\left(\frac{v_{0,\theta} + u_0}{r}\right) \\ A\left(\frac{u_{0,\theta} + v_0}{r} + v_{0,r}\right) \end{Bmatrix} - \int_{-h/2}^{h/2} \begin{Bmatrix} e_{31} \\ e_{31} \\ 0 \end{Bmatrix} E_z dz \quad (22)$$

$$\begin{Bmatrix} N_{r1} \\ N_{\theta1} \\ N_{r\theta1} \end{Bmatrix} = \frac{1}{1-\nu^2} \begin{bmatrix} 1 & \nu & 0 \\ \nu & 1 & 0 \\ 0 & 0 & \frac{1-\nu}{2} \end{bmatrix} \begin{Bmatrix} Au_{1,r} - Cw_{1,rr} \\ A\left(\frac{v_{1,\theta} + u_1}{r}\right) - C\left(\frac{rw_{1,\theta} + w_{1,\theta\theta}}{r^2}\right) \\ A\left(\frac{u_{1,\theta} - v_1}{r} + v_{1,r}\right) - 2C\left(\frac{rw_{1,r\theta} - w_{1,\theta}}{r^2}\right) \end{Bmatrix} \quad (23)$$

4.0 BOUNDARIES OF INSTABILITY REGIONS

Considering the axisymmetric dynamic stability of the plate, and are the pre-buckling forces that must be calculated form an equilibrium analysis of the plate, therefore

$$N_{r0} = N_{\theta0} = -p_r, \quad N_{r\theta0} = 0 \quad (24)$$

With this condition, the first and third dynamic stability Equation (21) become

$$\begin{aligned} & \frac{A}{1-\nu^2} \left(\frac{d^2u_1}{dr^2} + \frac{du_1}{rdr} - \frac{u_1}{r} \right) + \frac{C}{1-\nu^2} \left(-\frac{d^3w_1}{dr^3} - \frac{d^2w_1}{rdr^2} + \frac{dw_1}{r^2dr} \right) = 0 \\ & \frac{B}{1-\nu^2} \nabla^4 w_1 + \left(p_r - \int_{-h/2}^{h/2} e_{31} E_z dz \right) \nabla^2 w_1 + \frac{C}{1-\nu^2} \left(\frac{du_1}{r^2dr} - \frac{u_1}{r^3} - \frac{2d^2u_1}{rdr^2} - \frac{d^3u_1}{dr^3} \right) + w_{1,tt} \int_{-h/2}^{h/2} \rho dz = 0 \end{aligned} \quad (25)$$

Making

$$\frac{dw_1}{dr} = Y, \quad \frac{d^2w_1}{dr^2} = \frac{dY}{dr} = Y', \quad \frac{d^3w_1}{dr^3} = \frac{d^2Y}{dr^2} = Y'' \quad (26)$$

and

$$q = \frac{A}{1-\nu^2} u_1 - \frac{C}{1-\nu^2} Y \quad (27)$$

and substituting Equations (26) and (27) in the first stability Equation (25), we find

$$rq'' + rq' - q = 0 \tag{28}$$

The solution of Equation (28) is

$$q = c_1 r + c_2 / r \tag{29}$$

The boundary conditions for clamped edge are

$$\begin{aligned} u_1 = \frac{dw_1}{dr} &= \text{finite} & \text{at} & \quad r = 0 \\ u_1 = \frac{dw_1}{dr} &= 0 & \text{at} & \quad r = R \end{aligned} \tag{30}$$

Applying the boundary conditions to Equation (29) yields

$$\begin{aligned} c_1 &= 0 & , & \quad c_2 = 0 \\ q &= 0 \end{aligned} \tag{31}$$

the value of $q = 0$ is set in Equation (27), and solved for u_1 to give

$$u_1 = \frac{C}{A} \frac{du_1}{dr} \tag{33}$$

The solution for u_1 from Equation (33) is set in the second Equation (25), then the axisymmetric dynamic stability equations of FG piezoelectric circular plate can be expressed as

$$\nabla^4 w_1 + \left(p_r - \int_{-h/2}^{h/2} e_{31} E_z dz \right) \nabla^2 w_1 + M w_{1,tt} = 0 \tag{34}$$

where

$$D = \frac{B}{1-\nu^2} - \frac{C}{A(1-\nu^2)} \quad , \quad M = \int_{-h/2}^{h/2} \rho dz \tag{35}$$

Solutions of the dynamic stability equation are assumed to be in the following form:

$$w_1 = f(t)\varphi(r) \tag{36}$$

where

$$\psi(r) = I_n(\lambda R)J_n(\lambda r) - J_n(\lambda R)I_n(\lambda r) \tag{37}$$

then the solution is satisfied the boundary conditions

$$w_1 = \frac{dw_1}{dr} = 0 \quad \text{at} \quad r = R \tag{38}$$

and the natural frequency equation

$$D\nabla^4\psi - M\varpi^2\psi = 0 \tag{39}$$

where $n=0,1,2,3,\dots$, $J_n(x)$ and $I_n(x)$ are the Bessel function of first type and first modified Bessel functions of first type, respectively. λR are the roots of frequency equation

$$J_n(\lambda R)\frac{dI_n(\lambda R)}{dr} - \frac{dJ_n(\lambda R)}{dr}I_n(\lambda R) = 0 \tag{40}$$

The natural frequencies are related to these roots by

$$\varpi^2 = \frac{\lambda^4 D}{M} \tag{41}$$

Substitution of Equations (2), (36), (37) and (41) into Equation (34) yields

$$M\psi \frac{d^2 f}{dt^2} + \left\{ \varpi^2 M\psi + \left[\left(p_0 - \int_{-h/2}^{h/2} e_{31} E_{z0} dz \right) + \left(p_r - \int_{-h/2}^{h/2} e_{31} E_{zt} dz \right) \cos \omega t \right] \nabla^4 \psi \right\} f = 0 \tag{42}$$

Multiply the item $\psi(r)rdr$ in Equation (42), and integral along the whole plate, obtains following differential equations set:

$$\frac{d^2 f}{dt^2} + \varpi_a^2 (1 - 2\mu_a \cos \omega_a t) f = 0 \tag{43}$$

where

$$\begin{aligned} \bar{\omega}_a^2 &= \bar{\omega}^2 \left[1 - \frac{\int_{-h/2}^{h/2} e_{31} E_{z0} dz}{p_{cr}} \right], \mu_a = \left(p_r - \frac{\int_{-h/2}^{h/2} e_{31} E_{zt} dz}{-h/2} \right) / 2 \left(p_{cr} - p_0 + \frac{\int_{-h/2}^{h/2} e_{31} E_{z0} dz}{-h/2} \right) \\ p_{cr} &= - \frac{\int_0^R \int_0^{2\pi} \psi^2 r dr d\theta}{\int_0^R \int_0^{2\pi} \psi \psi r dr d\theta} M \psi^2 = \frac{\int_0^R \int_0^{2\pi} [J_n(\lambda R) J_n(\lambda r) - J_n(\lambda R) I_n(\lambda r)]^2 r dr d\theta}{\int_0^R \int_0^{2\pi} \lambda^2 [J_n(\lambda R) J_n^2(\lambda r) - J_n^2(\lambda R) I_n^2(\lambda r)]^2 r dr d\theta} M \psi^2 \end{aligned} \quad (44)$$

Equation (43) is well-known Mathieu equation μ_a is the excitation parameter, and $\bar{\omega}_a$ is the free vibration frequency of the plate loaded by constant radial force and electric field. p_{cr} is the Euler buckling load. ω_a express the boundary frequencies of the instability regions. Equation (43) is a system of second-order differential equations with periodic coefficients of the Mathieu type. Its periodic solution can be obtained through the Bolotin’s method (Bažant et al., 2010). The stability boundaries can be constructed by periodic solutions of periods T and $2T$, where $T = 2\pi/\omega$. In general, the solutions with period $2T$ are dominating. A first order approximation to the solution with periodicity $2T$ can be derived in the form of

$$f(t) = \{a\} \sin(\omega t/2) + \{b\} \cos(\omega t/2) \quad (45)$$

where $\{a\}$ and $\{b\}$ are arbitrary vectors. To determine the boundaries of the principal instability region, we substitute $f(t)$ of Equation (45) into (43) and then set the first-order determinant to obtain the following result:

$$\omega_a^2 = 4\bar{\omega}_a^2(1 - \mu_a) \quad , \quad \omega_a^2 = 4\bar{\omega}_a^2(1 + \mu_a) \quad (46a,b)$$

Equation (46) is referred to as the equation of boundary frequencies. It is used to dictate the dynamic stability of the FG piezoelectric plate and calculate the boundaries of instability regions.

5.0 RESULTS AND DISCUSSION

Axisymmetric stability of a piezoelectric circular plate made of functionally graded microstructure is considered. The edge boundary conditions are clamped. The state of periodic load is the uniform pulsating radial compressive load and electric field in the out-plane direction, which may be defined as

$$\begin{aligned} p_r(t) &= p_0 + p_t \cos \omega t = \alpha p_{cr} + \beta p_{cr} \cos \omega t \\ E_z(t) &= E_{z0} + E_{zt} \cos \omega t \end{aligned} \tag{47}$$

where α is the static load factor, and β is the dynamic load factor. In the following, let $\beta = 0.5$, The material properties of the FG piezoelectric plate are listed in Table 1 some of which can be directed by the reference (Takagi et al., 2002). If there is no statement in the following discuses, the materials distribution of the plate is from PZT/30%Pt to PZT from top to bottom. Results on the dynamic instability frequencies for different cases are given in Table 2, where, ω_{a1}^2 and ω_{a2}^2 correspond to the frequencies dictated by Equations (46a) and (46b), respectively, and ω_{a0}^2 express the free vibration frequency of the plate. Figure 1 is the sketch map of the frequency unstable region. The applied periodic voltage gives rise to an average electric field in the radial direction.

Table1. Density, elastic and piezoelectric constants for the PZT/Pt material (Takagi et al., 2002)

| | $\rho(\text{kg/m}^3)$ | E(Gpa) | $e_{31}(\text{C/m}^2)$ | ξ_{11}/ξ_0 | ξ_{33}/ξ_0 |
|--------------------------|-----------------------|--------|------------------------|------------------|------------------|
| $p_u(\text{PZT})$ | 790 | 69.64 | -16.8 | 1654 | 1924 |
| $p_b(\text{PZT}/30\%Pt)$ | 1187 | 153.77 | 0 | 0 | 0 |

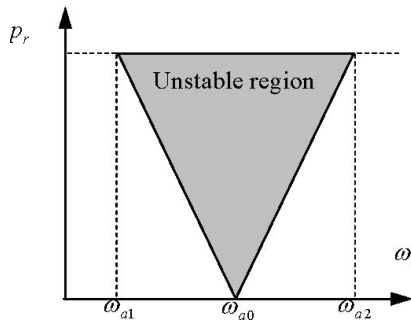


Figure 1. Sketch map of the unstable region in the frequency domain

It is seen from Table 2 that as the static electric field can make the unstable regions move to higher or lower frequency region, and the dynamic electric field can reduce or expand the unstable region. The positive electric field can make the structure unstable and the negative electric field can decrease the effect. With Table 2, the results show the positive electric field reduces the unstable region and the negative electric field expands it, but the converse piezoelectric effects have slight effect on the unstable region. Notice that the coercive electric field for most piezoelectric ceramic is of order 10^6 V/m; we can conclude that the

electric field (always less than 10^6 V/m in the applications) alone can only slightly affect the unstable region.

Figure 2 shows the buckling load p_c versus volume fraction exponent n for $h/R = 0.04, 0.08,$ and 0.1 , the materials of the top and bottom surfaces of the plate are PZT/30%Pt and PZT, respectively. As it can be seen the volume fraction exponent n of FG plate affects the critical buckling load and as n increases, the buckling load of the FG plate increases. This effect is dominant for higher h/R s. It is also shown that as h/R increases, the buckling load of the FG plate increases for all values of volume fraction exponents.

Figure 3 shows the buckling load p_c versus volume fraction exponent n for two case of components of the plate are exchange from PZT/30%Pt to PZT along top to bottom for $h/R = 0.1$ and vice versa. The value of the exponent n is varied between 0 and 10. It is seen that the buckling load the mechanical instability of FGM piezoelectric plate is lower than that for fully PZT/30%Pt plates, but upper than fully PZT plates.

Table 2. The unstable region of frequency rate ω_a/ϖ , with the cases $(h = 0.1, R = 1, \beta = 0.5)$

| Model | Electric field | Frequency ratio | $n = 0$ | $n = 1$ | $n = 2$ | $n = 3$ |
|---------|------------------------------------|----------------------|---------|---------|---------|---------|
| $M = 0$ | $E_{z_0} = 0$ $E_{z_1} = 0$ | ω_{a1}/ϖ | 3 | 3 | 3 | 3 |
| | | ω_{a0}/ϖ | 4 | 4 | 4 | 4 |
| | | ω_{a2}/ϖ | 5 | 5 | 5 | 5 |
| | $E_{z_0} = 10^6$ $E_{z_1} = 0$ | ω_{a1}/ϖ | 2.930 | 2.977 | 2.986 | 2.990 |
| | | ω_{a0}/ϖ | 3.930 | 3.977 | 3.986 | 3.990 |
| | | ω_{a2}/ϖ | 4.930 | 4.977 | 4.986 | 4.990 |
| | $E_{z_0} = -10^6$ $E_{z_1} = 0$ | ω_{a1}/ϖ | 3.070 | 3.023 | 3.014 | 3.010 |
| | | ω_{a0}/ϖ | 4.070 | 4.023 | 4.014 | 4.010 |
| | | ω_{a2}/ϖ | 5.070 | 5.023 | 5.014 | 5.010 |
| | $E_{z_0} = 0$ $E_{z_1} = 10^6$ | ω_{a1}/ϖ | .965 | 2.989 | 2.993 | 2.995 |
| | | ω_{a0}/ϖ | 4 | 4 | 4 | 4 |
| | | ω_{a2}/ϖ | 5.035 | 5.011 | 5.007 | 5.005 |
| | $E_{z_0} = 0$ $E_{z_1} = -10^6$ | ω_{a1}/ϖ | 3.035 | 3.011 | 3.007 | 3.005 |
| | | ω_{a0}/ϖ | 4 | 4 | 4 | 4 |
| | | ω_{a2}/ϖ | 4.965 | 4.989 | 4.993 | 4.995 |

| | | | | | | |
|------------------------------------|------------------------------------|----------------------|-------|-------|-------|-------|
| $M = 1$ | $E_{z_0} = 0$ $E_{z_1} = 0$ | ω_{a1}/ϖ | 3 | 3 | 3 | 3 |
| | | ω_{a0}/ϖ | 4 | 4 | 4 | 4 |
| | | ω_{a2}/ϖ | 5 | 5 | 5 | 5 |
| | $E_{z_0} = 10^6$ $E_{z_1} = 0$ | ω_{a1}/ϖ | 2.978 | 2.993 | 2.996 | 2.997 |
| | | ω_{a0}/ϖ | 3.978 | 3.993 | 3.996 | 3.997 |
| | | ω_{a2}/ϖ | 4.978 | 4.993 | 4.996 | 4.997 |
| | $E_{z_0} = -10^6$ $E_{z_1} = 0$ | ω_{a1}/ϖ | 3.022 | 3.007 | 3.004 | 3.003 |
| | | ω_{a0}/ϖ | 4.022 | 4.007 | 4.004 | 4.003 |
| | | ω_{a2}/ϖ | 5.022 | 5.007 | 5.004 | 5.003 |
| | $E_{z_0} = 0$ $E_{z_1} = 10^6$ | ω_{a1}/ϖ | 2.995 | 2.998 | 2.999 | 2.999 |
| | | ω_{a0}/ϖ | 4 | 4 | 4 | 4 |
| | | ω_{a2}/ϖ | 5.005 | 5.001 | 5.001 | 5.001 |
| $E_{z_0} = 0$ $E_{z_1} = -10^6$ | ω_{a1}/ϖ | 3.005 | 3.002 | 3.001 | 3.001 | |
| | ω_{a0}/ϖ | 4 | 4 | 4 | 4 | |
| | ω_{a2}/ϖ | 4.995 | 4.998 | 4.999 | 4.999 | |

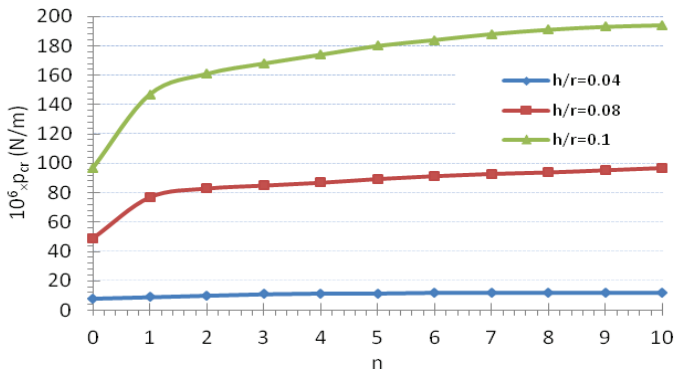


Figure 2. Buckling load p_{cr} of the different volume fraction exponent n with the cases ($m = 0, \alpha = 0, h/R = 0.1, h/R = 0.08, h/R = 0.04$)

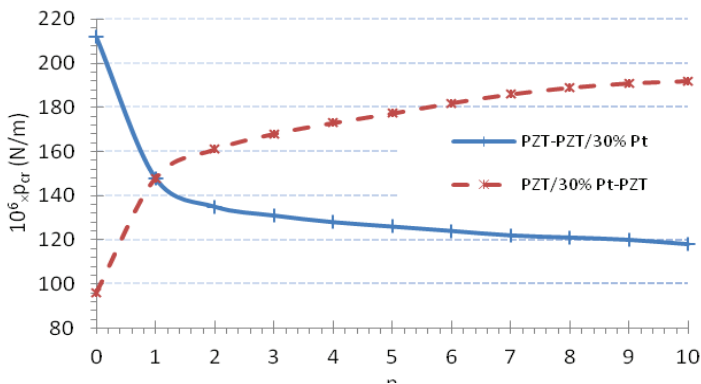


Figure 3. Buckling load p_{cr} of the different volume fraction exponent n of reverse components of FG with the cases ($m = 0, h/R = 0.1,)$

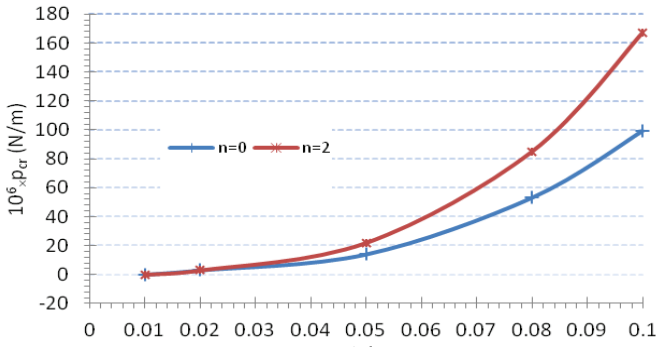


Figure 4. Buckling load p_{cr} of the different thickness with the cases ($m = 0, h/R = 0.1, \alpha = 0, n = 0, 2$)

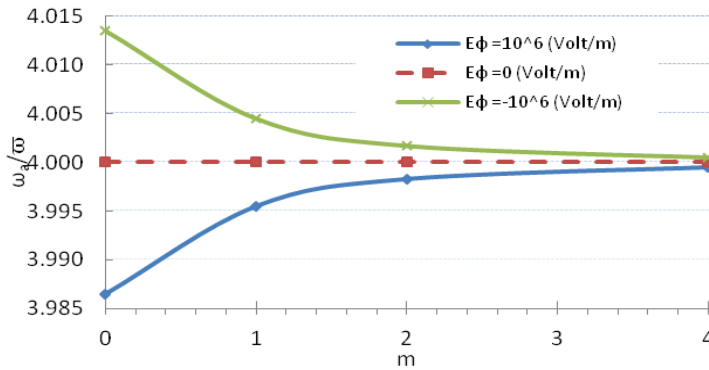


Figure 5. Free vibration frequency rate ω_a/ω under different model m , with the cases ($n = 2, h/R = 0.1, \alpha = 0$)

Figure 4 shows the buckling load p_{cr} versus thickness of plate (h) for various values of the volume fraction exponent ($n = 0, 2$) for the clamped edges. It is observed that as the values of (h) increases, the buckling load increases. Figure 5 shows the effect of different models on free vibration frequency rates of FG piezoelectric circular plate for three electric fields. It is seen that the effect of the electric field on variation of vibration frequency rates become faintness when the model number increases. Figure 6 shows the free vibration frequency rate versus static loads p_0 for $m = 2, n = 2$ and $h/R = 0.1$. The obtained results reveal that the thickness of the plate can change the free vibration frequency largely; on the contrary, the effect of electric field is negligible.

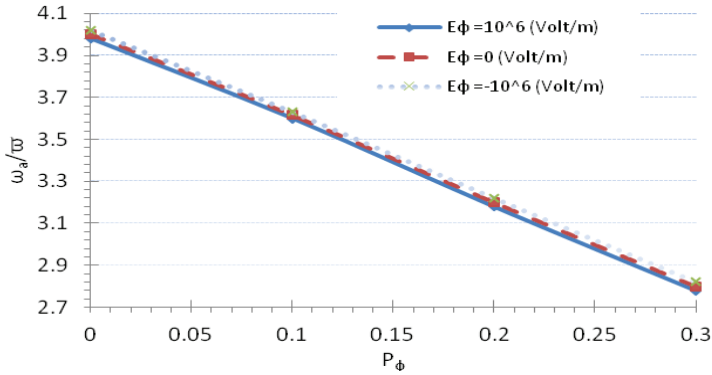


Figure 6. Free vibration frequency rate under different mechanical loads with the cases ($m = 2, n = 2, h/R = 0.1$)

Figure 7 illustrates the effects of volume fraction exponent n on the free vibration frequency rate, where $m = 0, h/R = 0.1$ and $\alpha = 0$. We can see that the effect of electric is decrease as the larger value of k is increase.

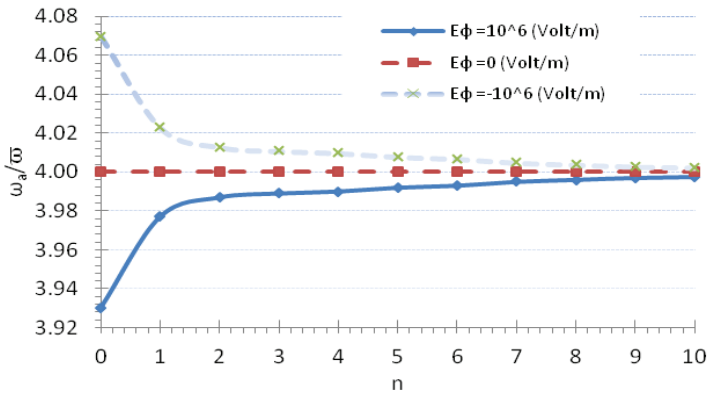


Figure 7. Free vibration frequency rate ω_a/ω of volume fraction exponent n under the different electric field with the cases ($m = 0, h/R = 0.1, \alpha = 0$)

6.0 CONCLUSIONS

Based on Love-Kirchhoff hypothesis, the Sander's non-linear strain-displacement relation and variational formulation the dynamic stability analysis of piezoelectric circular plate made of functional graded microstructure is presented. The plate is subjected to a radial loading and electric field in the normal direction. After deriving the Mathieu-Hill equations governing the instability problem, the Bolotin's method is employed to obtain the dynamic instability regions. Obtained results

show that the piezoelectric effect only slightly affects the unstable region whilst the functionally graded composite materials plays a significant role in changing the unstable regions and the buckling loads. So the designer should consider the component of the FG piezoelectric rather than the piezoelectric effect.

ACKNOWLEDGEMENT

The author is grateful for the financial support as a grant from International University of Imam Khomeini.

REFERENCES

- Bažant, Z. P. & Cedolin, L. (2010). *Stability of structures: elastic, inelastic, fracture and damage theories*. World Scientific Publishing Company.
- Bodner, V. A. (1938). Stability of plates under the action of periodic force, *Prikladnaya Matematika I Mekhanika*, 2, 87–94 (in Russian).
- Ebrahimi, F. (2013). Analytical investigation on vibrations and dynamic response of functionally graded plate integrated with piezoelectric layers in thermal environment. *Mechanics of Advanced Materials and Structures*, 20(10), 854–870.
- Ebrahimi, F. & Rastgoo, A. (2008a). An analytical study on the free vibration of smart circular thin FGM plate based on classical plate theory. *Thin-Walled Structures*, 46(12), 1402–1408
- Ebrahimi, F. & Rastgoo, A. (2008b). Free vibration analysis of smart annular FGM plates integrated with piezoelectric layers. *Smart Materials and Structures*, 17(1), 015044.
- Ebrahimi, F., Rastgoo, A., & Atai, A. A. (2009). A theoretical analysis of smart moderately thick shear deformable annular functionally graded plate. *European Journal of Mechanics-A/Solids*, 28(5), 962–973.
- Ebrahimi, F., Rastgoo, A., & Kargarnovin, M. H. (2008). Analytical investigation on axisymmetric free vibrations of moderately thick circular functionally graded plate integrated with piezoelectric layers. *Journal of Mechanical Science and Technology*, 22(6), 1058–1072.
- Efraim, E., & Eisenberger, M. (2007). Exact vibration analysis of variable thickness thick annular isotropic and FGM plates. *Journal of Sound and Vibration*, 299(4), 720–738.
- Fakhari, V., Ohadi, A., & Yousefian, P. (2011). Nonlinear free and forced vibration behavior of functionally graded plate with piezoelectric layers in thermal environment. *Composite Structures*, 93(9), 2310–2321.

- Hosseini-Hashemi, S., Fadaee, M., & Atashipour, S. R. (2011). A new exact analytical approach for free vibration of Reissner–Mindlin functionally graded rectangular plates. *International Journal of Mechanical Sciences*, 53(1), 11–22.
- Khorshidvand, A. R., Jabbari, M., & Eslami, M. R. (2012). Thermoelastic buckling analysis of functionally graded circular plates integrated with piezoelectric layers. *Journal of Thermal Stresses*, 35(8), 695–717.
- Koizumi, M. (1993). The concept of FGM. In: Holt, J. B.; Koizumi, M.; Hirai, T.; Munir, Z. A. (ed.), *Ceramic Transactions*, Vol. 34, *Functionally Gradient Materials*, pp. 3–10. Westville: American Ceramic Society.
- Lee, H. J. (2005). Layerwise laminate analysis of functionally graded piezoelectric bimorph beams. *Journal of Intelligent Material Systems and Structures*, 16, 365–371.
- Loja, M. A. R., Soares, M., & Barbosa, J. I. (2013). Analysis of functionally graded sandwich plate structures with piezoelectric skins, using B-spline finite strip method. *Composite Structures*, 96, 606–615.
- Love, A. E. H. (2013). *A treatise on the mathematical theory of elasticity*. Cambridge University Press.
- Matsunaga, H. (2008). Free vibration and stability of functionally graded plates according to a 2-D higher-order deformation theory. *Composite Structures*, 82(4), 499–512.
- Takagi, K., Li, J. F., Yokoyama, S., Watanabe, R., Almajid, A., & Taya, M. (2002). Design and fabrication of functionally graded PZT/Pt piezoelectric bimorph actuator. *Science and Technology of Advanced Materials*, 3(2), 217–224.
- Yamaguchi, D., Kanda, T., Suzumori, K., Fujisawa, K., Takegoshi, K., & Mizuno, T. (2013). Ultrasonic motor using two sector-shaped piezoelectric transducers for sample spinning in high magnetic field. *Journal of Robotics and Mechatronics*, 25, 384–391.
- Zhao, C. (2011). *Ultrasonic motors: technologies and applications*. Springer.
- Zhao, X., Lee, Y. Y., & Liew, K. M. (2009). Free vibration analysis of functionally graded plates using the element-free kp-Ritz method. *Journal of Sound and Vibration*, 319, 918–939.
- Zhu, X. H. & Meng, Z. (1995). Operational principle, fabrication and displacement characteristics of a functionally gradient piezoelectric ceramic actuator. *Sensors and Actuators A*, 48, 169–176.

